A Broadband Dual-Antenna Pair Based on Half-Open Cavity With Horizontally Polarized Radiation for Wi-Fi 6/6E Application

Xiaopeng Zhang, Libin Sun, *Member, IEEE*, Yue Li, *Senior Member, IEEE*, and Zhijun Zhang, *Fellow, IEEE*

***Abstract*— A broadband and omnidirectional coverage dual-antenna pair with horizontally polarized (HP) radiation for Wi-Fi 6/6E application is presented in this article. The dual-antenna pair is composed of two open cavity antennas (OCA) with the apertures partially sealed. By sealing the aperture partially, the dimension of the proposed half-OCA (HOCA) is reduced dramatically without changing the matching bandwidth and the radiation performance. Compared with other OCAs with the omnidirectional radiation, the proposed dual-antenna pair realizes omnidirectional coverage in azimuth plane by the back-to-back combination of two unidirectional OCAs, which also makes the antenna have multiple-input multiple-output (MIMO) performance. Besides, a broadband covering both 5 and 6 GHz bands of Wi-Fi 6/6E is also achieved. A prototype was fabricated and tested to validate the concept. In well agreement with the simulated results, the measured bandwidth with $S_{11} < -10$ dB for two ports are 5.03–7.35 GHz and 5.09–7.53 GHz, respectively, with the isolation higher than 22.67 dB. Besides, the measured gain > 5 dBi and ECC < 0.05 are achieved over the operating band. The proposed antenna shows great potential in the Wi-Fi 6/6E application.**

***Index Terms*— Broadband, dual-antenna pair, MIMO, omnidirectional coverage, open cavity antenna (OCA), Wi-Fi 6/6E.**

I. Introduction

IN MODERN wireless communication technology, Wi-Fi occupies an important position. With the development of Wi-Fi technology, wireless routers have entered more and more homes, offices, factories, etc., bringing people a fast and unrestricted Internet experience, and becoming one of the indispensable devices in people's daily life. Many Wi-Fi protocol standards are developed in history covering the 2.45 GHz (2.4–2.484 GHz) and 5 GHz (5.15–5.83 GHz) bands. Wi-Fi 6E is the latest extension of Wi-Fi 6 to the 6 GHz (5.925–7.125 GHz) band. The introduction of the 6 GHz band can effectively alleviate the congestion problem of other bands, which also brings the antenna design challenges because of such a wide bandwidth.

The routers with whip external antennas are the most common type in many application scenarios. The external antennas are often conventional monopoles and dipoles with vertically polarized (VP) radiation. However, it is a challenge for these two conventional antennas to cover such a wide 6 GHz band. Many approaches were applied for monopoles and dipoles to introduce multiple resonances and enhance the bandwidth to cover 2.45 and 5 GHz bands such as etching slot on the arm [1]–[3], adding parasitic patch [4]–[6] or *LC* resonator [7] and introducing choke elements or structures [8]. All these techniques are proved useful for constructing different resonant structures corresponding to different frequencies. However, whether the existing approaches can tackle the issue of the coverage for such a wide 6 GHz band is still uncertain. In comparison, ultrawideband (UWB) [9], [10] antennas could easily cover all the bands for Wi-Fi 6/6E, but a significant problem of the lack of horizontally polarized (HP) radiation is still unsolved.

For the conventional routers with vertical monopoles or dipoles with VP radiation as the external antennas, the HP radiation is natively lacking while HP antennas are very common in various devices. In daily communication scenarios, the native lack of HP radiation will cause the limitation in channel capacity. The polarization mismatch of the transmitter and receiver antennas can only be ameliorated by rich environmental scattering. Horizontal dipoles circle array is an effective means to realize azimuth plane coverage with HP radiation for the multiple-input multiple-output (MIMO) application. Many rotating dipole arrays were proposed with dipoles of different shapes [11], [12]. The dipoles are designed particularly with two pairs of arms for covering both 2.45 and 5 GHz bands and slits are introduced on the ground to suppress the mutual coupling for MIMO application. However, this type of antenna array is suitable for low profile router instead of the router with external antennas. Therefore, other types of antennas need to be investigated to realize HP radiation.

In addition to the lack of the HP radiation, the decoupling of two nearby VP elements is also a challenge. In general, more antennas are required for router to cover the new band.

Manuscript received June 29, 2021; revised November 24, 2021; accepted December 19, 2021. Date of publication January 13, 2022; date of current version June 13, 2022. This work was supported by the National Natural Science Foundation of China under Contract 61971254. *(Corresponding author: Zhijun Zhang.)*

The authors are with the Beijing National Research Center for Information Science and Technology (BNRist), Tsinghua University, Beijing 100084, China (e-mail: zjzh@tsinghua.edu.cn).

Color versions of one or more figures in this article are available at https://doi.org/10.1109/TAP.2022.3140322.

Digital Object Identifier 10.1109/TAP.2022.3140322

With the limitation of space, the more antennas, the closer the spacing. However, the mutual coupling effect of dipoles or monopoles would increase while the spacing is little, which will significantly degrade the antenna and MIMO performance. Plenty of decoupling structures and techniques have been investigated to suppress the mutual coupling of two closely spaced antennas [13]–[15], but they are often not universal. Decoupling network is an effective and universal structure for the decoupling of antennas [16]–[17], but the networks are often very complicated with a large size. In [18], a general decoupling method based on common and differential modes cancellation was proposed. High isolation is achieved for two dipoles closely spaced only by simple neutralization lines and lumped elements, but the decoupled bandwidth is quite narrow. Compared with the nearby dipoles or monopoles with VP radiation, the decoupling for two nearby open resonant cavity antennas (OCAs) with HP radiation is simple relatively.

OCA is a convenient structure for realizing HP radiation with omnidirectional or unidirectional pattern. Omnidirectional OCAs with HP radiation were realized in [19] and [20] based on impedance surface and partially reflective strip at the open sides, respectively, but the bandwidth is narrow. In [21], it is proven that the resonant frequencies of modes could be adjusted by the length of the cavity. However, the 3rd mode is suppressed for preventing beam tilt, so the bandwidth is narrow too. Broadband was achieved in [22] with unidirectional pattern by introducing shorting vias around the trisecting lines of the cavity to make the resonant frequencies of the 1st and 3rd modes closer to each other, but a large ground is needed. In [23], a HP omnidirectional antenna with cavity configuration was proposed covering the 2.45 and 5 GHz bands for Wi-Fi application. However, different from other antennas above, the omnidirectional radiation is realized by horizontal current loops on the top and bottom slots and the dual resonance corresponds to two different slot modes. Besides, the feeding structure is complicated and unstable.

To tackle the exist problems in the current router antennas and satisfy the demand of Wi-Fi 6/6E application, a dual-antenna pair operating in 5 and 6 GHz bands with HP radiation and omnidirectional coverage in azimuth plane is proposed in this article. The proposed dual-antenna pair is composed of two back-to-back half-open cavity antennas (HOCAs) with the apertures partially sealed and each of them covers half azimuth plane. Similar with the monopole and dipole, the proposed antenna also has whip configuration which is suitable for applying as external antennas on conventional routers. Besides, the proposed antenna could complement HP radiation for current routers improving the channel capacity and reliability. Moreover, compared with the omnidirectional OCAs above [19]–[23], the amount of antenna can be doubled while occupying the same space, which means a significant improvement in MIMO performance.

II. Broadband Half-Open Cavity Antenna

Fig. 1(a) is the configuration of the proposed dual-antenna pair which is a back-to-back combination of two HOCAs. The radiation apertures are opposite for omnidirectional coverage and two ports are also placed in different faces. The single HOCA shown in Fig. 1(c) is a cuboid metal cavity with only one side open. Two symmetrical metal sheets extend inward from both sides with width of T changing the size of the open aperture. The yellow metal probe is used to excite the cavity. A circle slot is etched on the back side, to adjust the impedance matching. The dimension of the single HOCA is $0.2\ \lambda_0 \times 0.12\lambda_0 \times 1.2\lambda_0$ at 6 GHz which is half of the dual-antenna pair.

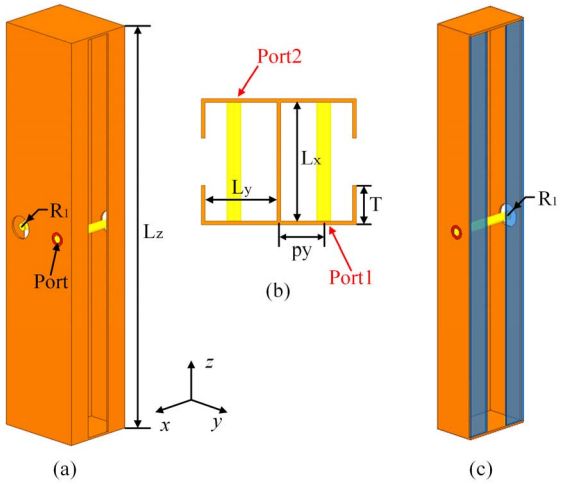

Fig. 1. Geometry of the proposed dual-antenna pair. (a) Perspective view. (b) Top view without top and bottom sheets. (c) Single HOCA element. $L_z = 60$ mm, $L_x = 10$ mm, $L_y = 6$ mm, $R_1 = 1.7$ mm, $T = 3$ mm, $py = 3.5$ mm.

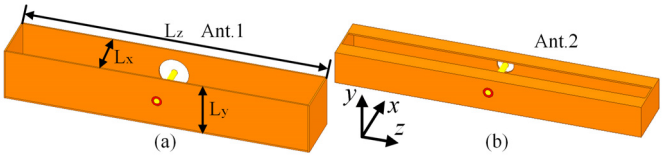

Fig. 2. Design process of the single antenna. (a) Ant. 1. (b) Ant. 2 (The proposed half-open cavity antenna).

TABLE I
Design Process of the Proposed HOCA

Dimensions (mm)		*Lx*	*Ly*	*Lz*
Ant. 1	Case I*	2	10	100
	Case II	10	10	100
	Case III	10	10	60
Ant. 2	Case IV	10	6	60

* Ant. 1 in Case I is not matched

The design process of the proposed single HOCA is illustrated in Fig. 2 and Table I. At first, the Ant. 1 in Case I is simulated without matching. The simulated resonant frequencies of the 1st mode ($TE_{0,1/2,1}$ mode, f_{1st}) and the 3rd mode ($TE_{0,1/2,3}$ mode, f_{3rd}) are 6.5 and 7.8 GHz, respectively, as shown in Fig. 3(a). The resonant frequencies could also be calculated by

$$\left(\frac{\pi}{2L_y}\right)^2 + \left(\frac{\pi}{L_z}\right)^2 = k_{1st}^2 \tag{1}$$

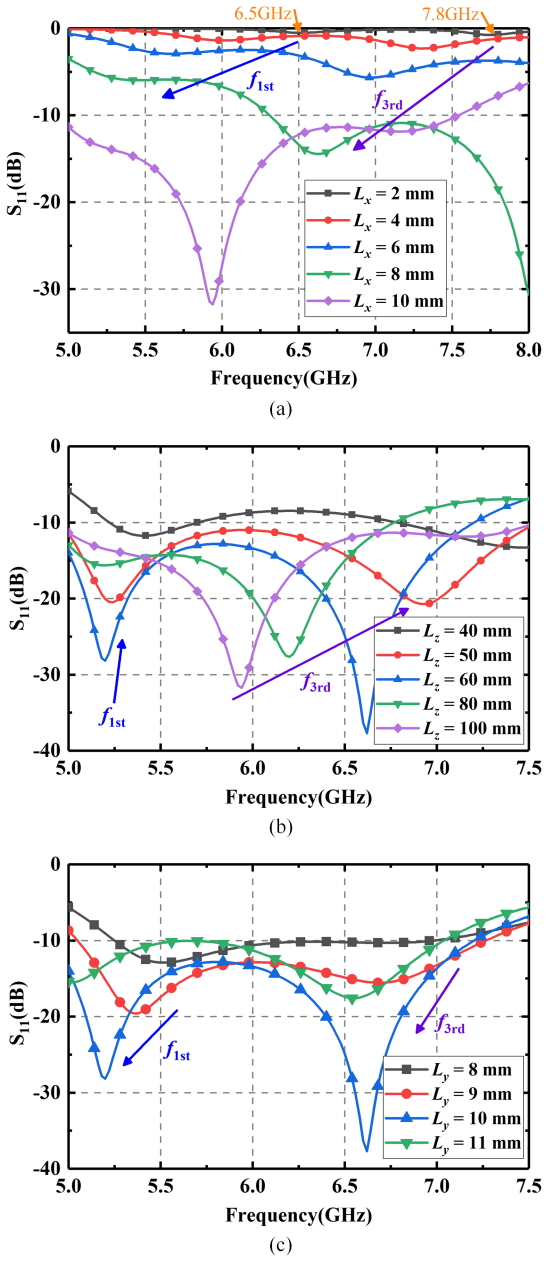

Fig. 3. Simulated S_{11} versus (a) width L_x in Case I. (b) Height L_z in Case II. (c) Length L_y in Case III.

$$\left(\frac{\pi}{2L_y}\right)^2 + \left(\frac{3\pi}{L_z}\right)^2 = k_{3rd}^2 \tag{2}$$

where k is the wavenumber in free space. Considering that the open side is not a perfect magnetic condition with part of the field extending out of the cavity, $L_y = 12$ mm is adopted in equations. The calculated resonant frequencies f_{1st} and f_{3rd} are 6.4 and 7.7 GHz, respectively, which are approximately consistent with the simulated results. However, the bandwidth of a conventional OCA with small L_x is narrow because of a high Q, so it is hard to cover both 5 and 6 GHz bands. Besides, the radiation pattern of a thin metal cavity is omnidirectional with low gain in *xoy* plane which is unwanted.

To enhance the bandwidth of the OCA, the width L_x is enlarged. With the increasing of L_x, the field will extend farther out of the cavity, which is equivalent to the increasing

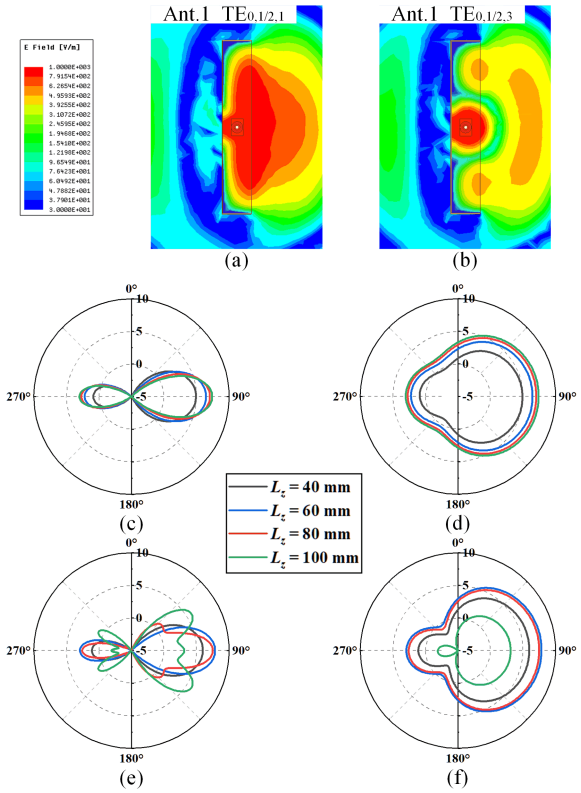

Fig. 4. Simulated magnitude of the E-field distribution of the Ant. 1 in *yoz* plane at (a) 5.2 GHz and (b) 6.6 GHz. Simulated radiation patterns versus L_z at 5.2 GHz in (c) *yoz* plane and (d) *xoy* plane; at 6.6 GHz in (e) *yoz* plane and (f) *xoy* plane.

of L_y. Therefore, the width L_x also has impact on the resonant frequencies even if not included in (1) and (2). As shown in Fig. 3(a), the resonant frequencies f_{1st} and f_{3rd} both decreases and get closer with the increasing of L_x, which is coincident with the discussion above. A width bandwidth covering both two bands is realized when $L_x = 10$ mm and the Ant.1 in Case II is obtained. However, the beam of Ant.1 in Case II will splits in high frequency because of the 3rd mode as shown in green line in Fig. 4(c) and (e).

To prevent the beam splitting in high frequency, the length L_z is decreased. Fig. 4(e) shows that the beam gradually became syncretic with the decreasing of L_z. Meanwhile, the resonant frequency f_{3rd} rises dramatically with the resonant frequency f_{1st} almost unchanged as shown in Fig. 3(b). The wideband is obtained with two strong resonances when $L_z = 60$ mm. Therefore, $L_z = 60$ mm is adopted in consideration of both the gain in *xoy* plane and bandwidth and the Ant.1 in Case III is designed. The resonant modes and radiation characteristics at two resonant frequencies are analyzed in detail in Fig. 4 as follows. The magnitude of the *E*-field distribution in *yoz* plane at 5.2 and 6.6 GHz when $L_z = 60$ mm are shown in Fig. 4. At low resonant frequency, the *E*-field of the 1st mode is observed in Fig. 4(a) with an obvious radiation and the radiation patterns are shown in Fig. 4(c) and (d). With the increasing of L_z, the gain increases slightly because of the enlargement of the radiation aperture. However, at high resonant frequency, both the 1st mode and the 3rd mode exist. It is distinct in Fig. 4(b) that the energy has already radiated

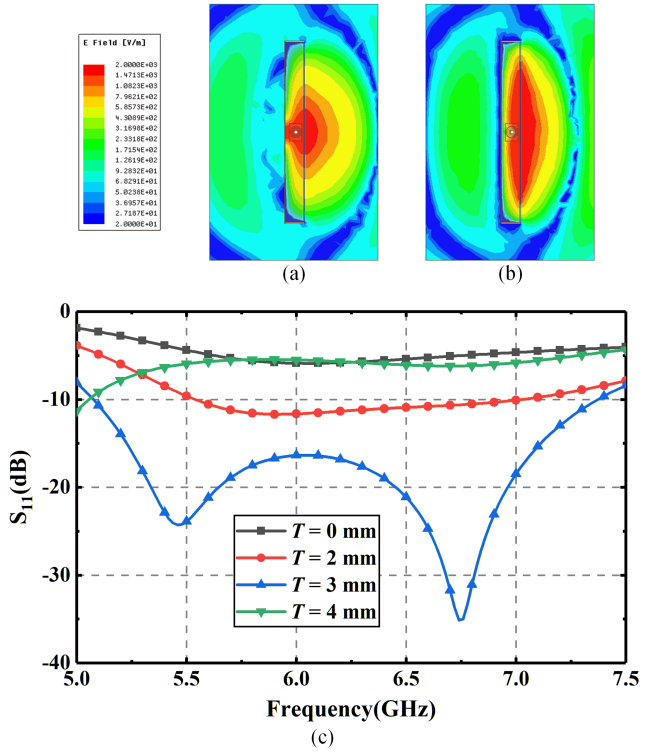

Fig. 5. Simulated magnitude of the E-field distribution of the Ant. 2 at 6 GHz when $L_y = 6$ mm. (a) without the sheets. (b) With the sheets and $T = 3$ mm. (c) Simulated S_{11} versus T.

to the space as the form of the 1st mode before the 3rd mode is observed, which means the opposite field of the 3rd mode is partly canceled out by that of the 1st mode. Therefore, the pattern of the 3rd mode does not distort when $L_z = 60$ mm in Fig. 4(e). As shown in Fig. 4(f), the radiation patterns of the Ant. 1 in Case III in *xoy* plane could realize a good 180° coverage with a high gain when L_z is appropriate.

For the application of the router external antennas, the Ant. 1 in Case III with the dimensions of 10 mm × 10 mm × 60 mm is too large. To finish the dimensions, we expect to reduce the width L_y of the Ant. 1 in Case III. However, as shown in Fig. 3(c), the impedance matching is poor when L_y is small. The magnitude of the E-field distribution of the Ant. 1 in Case III with $L_y = 6$ mm at 6 GHz is shown in Fig. 5(a). It is illustrated in figure that the cavity resonant mode is not generated because of the quite narrow width. Only the probe radiates with a field distribution similar to that of a monopole.

To enhance the cavity resonance, two symmetrical metal sheets are added in the aperture and the proposed HOCA is obtained. By adding two sheets, the Ant. 2 is more closed than the Ant. 1 reducing the direct contact between the probe and the free space which conduces to fully excite the cavity resonant mode. As shown in Fig. 5(b), the E-field is more concentrated in the cavity and between the sheets and radiates to the free space through the aperture, which is similar with that of the conventional cavity. Fig. 5(c) shows the impedance matching curves versus the width of the sheet. As the width T increases, the cavity resonance gradually generates and a broadband is obtained. But, if the width T is too large, the impedance matching will worsen, because the aperture is too narrow to radiate the energy effectively. Finally, $T = 3$ mm is adopted for a broadband impedance matching and the width of the aperture is 4 mm meanwhile. From other point of view, the Ant. 2 could be regarded as the Ant. 1 (Case III) with the side wall bended. For the Ant. 2, the sum of the width of the side wall and the metal sheet are approximately equal to that of the Ant. 1 (Case III). Therefore, the Ant. 2 has a similar resonance characteristic as the Ant. 1 (Case III) with a broad operating band and a similar radiation pattern. The radiation pattern of the Ant. 2 with 180° coverage in azimuth plane will be shown in Section III.

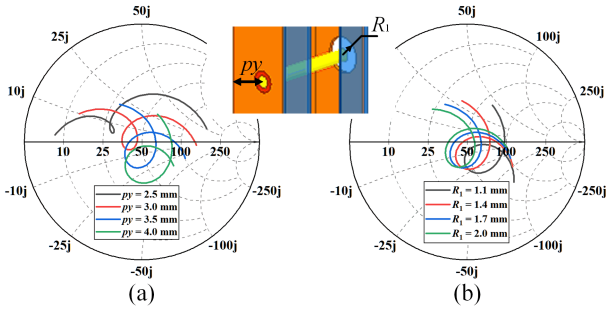

Fig. 6. Smith charts of impedance matching versus (a) *py* and (b) R_1.

The impact of the feeding position *py* and the radius R_1 of the circle slot are studied as shown in Fig. 6. The feeding position *py* is a key parameter to adjust the impedance matching because of the exist of the left metal wall and right aperture. Also, the radius R_1 could be used to change the impedance slightly. Finally, $py = 3.5$ mm and $R_1 = 1.7$ mm are adopted for a wide impedance matching bandwidth.

In conclusion, a broadband covering both 5 and 6 GHz bands for Wi-Fi 6/6E application and the radiation pattern covering 180° in azimuth plane are achieved by the proposed antenna with an almost half dimension compared with the Ant. 1 (Case III). Nevertheless, the radiation coverage is not enough for the MIMO application.

III. Dual-Antenna Pair

The MIMO technology is widely implemented in Wi-Fi communication system. Omnidirectional antenna is often applied in router for receiving signals from different paths in rich scattering environmental. For 360° coverage in azimuth plane, a dual-antenna pair composed of two proposed HOCAs in Section II is designed as shown in Fig. 7. The dual-antenna pair is a back-to-back combination of the two HOCAs (marked by red and green dash lines, respectively) sharing a common intermediate vertical plate (in gray) as shown in Fig. 7(c). Two antennas are fed through Port1 and Port2 by SMA connectors, respectively and each of them radiates with a pattern covering opposite 180° in azimuth plane. Considering the difficulty of solder, the ports are placed on opposite faces. It is proven that placing the ports on the same face or opposite faces has almost no impact on the antenna performance as shown in Fig. 8(c). The dimension of the dual-antenna pair is $0.2\ \lambda_0 \times 0.24\lambda_0 \times 1.2\lambda_0$ at 6 GHz.

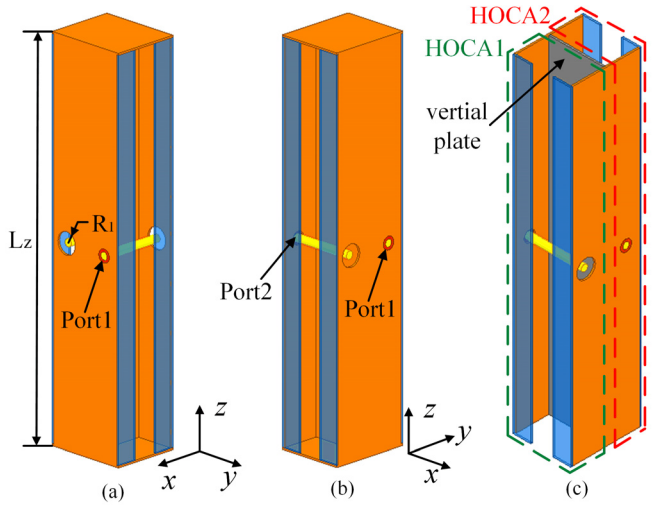

Fig. 7. Geometry of the proposed dual-antenna pair. (a) Perspective view. (b) Another perspective view. (c) Proposed dual-antenna pair without top and bottom sheets.

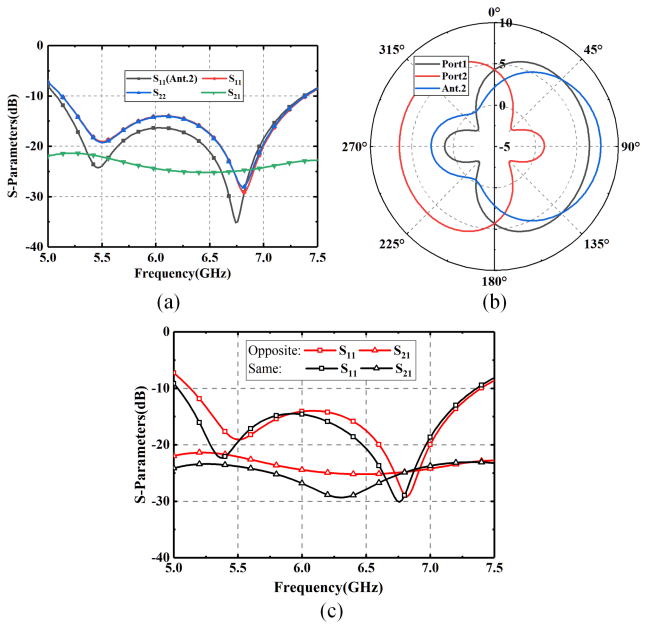

Fig. 8. Simulated (a) *S*-parameters and (b) radiation patterns of the dual-antenna pair. (c) Simulated *S*-parameters of the dual-antenna pair with different ports positions.

The simulated *S*-parameters of the dual-antenna pair and the Ant. 2 in Section II is shown in Fig. 8(a). The curves of impedance matching of these two antennas are extremely similar, which means that the connection has nearly no effect on the impedance matching. Besides, high isolation is achieved over the operating band with a distance only about 0.12 λ_0 in 6 GHz without complicated decoupling structures. The back-to-back connection technique makes the two HOCAs radiate toward the opposite directions, which improves the isolation directly. In addition, as shown in Fig. 9(a), when Port1 is excited, most of the energy is radiated forward with part of the energy propagating backward as surface wave along the side

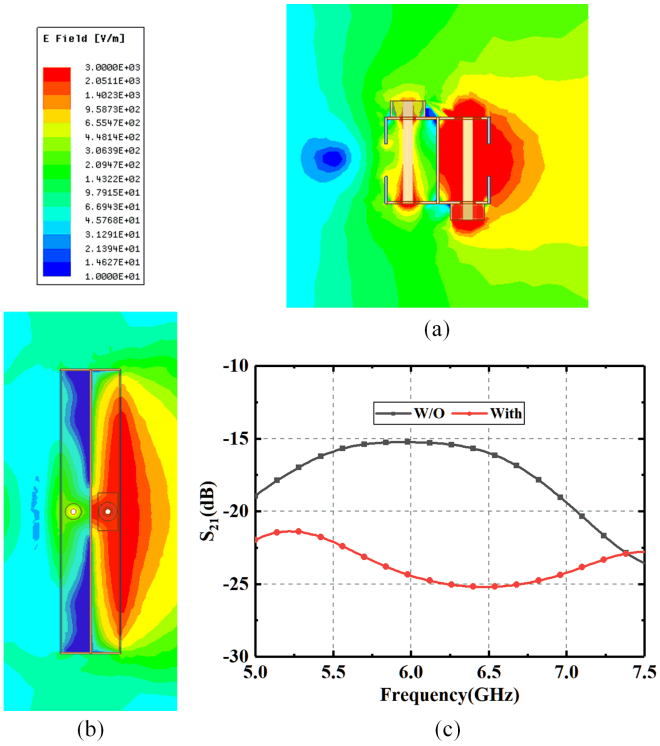

Fig. 9. Simulated complex magnitude of the *E*-field distribution of the dual-antenna pair when Port1 is excited (a) in *xoy* plane and (b) in *yoz* plane. (c) Simulated isolation with or without the top and bottom sheets.

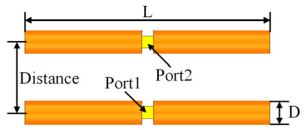

Fig. 10. Geometry of the dual-dipole pair.

wall. But the energy is finally radiated to the space instead of absorbed by Port2, so the isolation is high. Moreover, the top and bottom sheets also prevent the electromagnetic wave from diffracting from one cavity to the other at both ends which also contributes to the high isolation as shown in Fig. 9(b). It is proven in Fig. 9(c) that the isolation is improved acutely with the top and bottom sheets.

To demonstrate the advantage of our proposed dual-antenna pair, a comparison between dual-dipole pair and our proposed antenna is studied. As shown in Fig. 10, the dual-dipole pair is composed of two conventional dipoles without any extra decoupling structure. The dipole is metal cylinder with a diameter $D = 2$ mm and a length $L \approx 0.42\ \lambda_0$ in 6 GHz. As shown in Table II, the simulated isolation of dual-dipole pair is quite poor with a little distance. A simple decoupling method is proposed in [18] with isolation improved, but the bandwidth is still narrow. In comparison, our proposed dual-antenna pair has remarkable advantages in both bandwidth and isolation with a narrow distance.

The radiation patterns of the dual-antenna pair and the Ant. 2 are depicted in Fig. 8(b). The radiation pattern of one antenna of the dual-antenna pair slightly decreases in

TABLE II

COMPARISON OF THE PROPOSED DUAL-ANTENNA PAIR AND THE DUAL-DIPOLE PAIR

Item	Distance	Bandwidth	Isolation
Dual-dipole pair	0.12 λ_0	11.8%	> 4.6 dB
	0.24 λ_0	15.0%	> 8.4 dB
[18]	0.2 λ_0	8.7%	> 12 dB
Proposed dual-antenna pair	0.12 λ_0*	37.7%	> 21.4 dB

* The distance of our proposed dual-antenna pair is defined as the distance between the centers of two HOCAs.

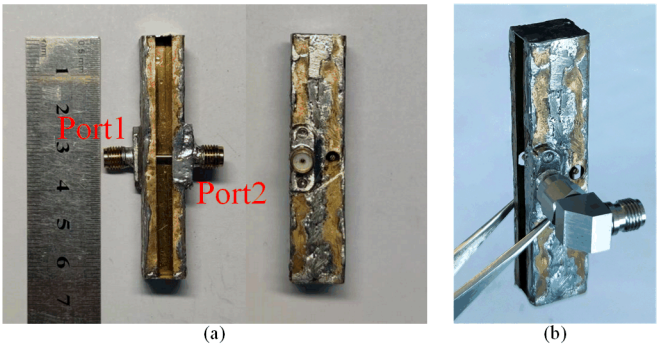

(a) (b)

Fig. 11. (a) Photograph of the proposed dual-antenna pair. (b) Proposed antenna with convertor.

forward and backward directions and increases in both side directions, which means that the new pattern is more suitable for realizing 180° coverage. This could be explained by the *E-field* distribution in *xoy* plane in Fig. 9(a). By combining two antenna elements, the side walls are equivalent to extending backward for each element. Therefore, more energy is radiated to the side directions before radiated backward while the surface wave transmits alone the side wall.

In conclusion, a dual-antenna pair with wide bandwidth, high isolation and better radiation patterns for omnidirectional coverage in azimuth plane is designed for the MIMO application.

IV. SIMULATED AND MEASURED RESULTS

An assembled prototype of the dual-antenna pair to verify the performance is shown is Fig. 11(a). The proposed dual-antenna pair is divided into five parts for manufacture, the front, back, top and bottom sheets, and the intermediate vertical plate. The symmetrical metal sheets in apertures are shaped by bending the front and back layers. All of them are made of brass plates ($\sigma = 1.5 \times 10^7$ S/m) with a thickness of 0.3 mm. Two ports are excited by SMAs with outer conductor soldered to the metal shell and inner conductor protruding into the cavity as what yellow metal stick shows in Fig. 7. Two ports are installed on different faces because it is difficult to solder two SMAs on the same face. When measuring, to weaken the influence of the feeding coaxial cable on the antenna radiation, a convertor was added on the antenna to switch the directions of the cable as shown in Fig. 11(b).

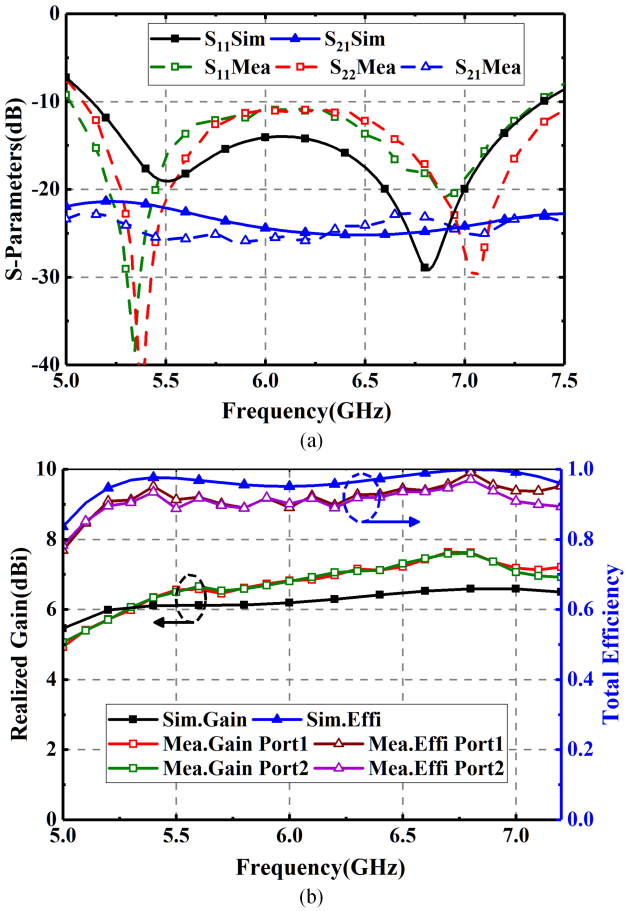

Fig. 12. Simulated and measured (a) *S*-parameters and (b) realized gains and total efficiencies of the dual-antenna pair.

A. S-Parameters

The simulated and measured reflection coefficients and isolation are reported in Fig. 12(a). The simulated S_{22} is almost identical with S_{11} because of the symmetrical construction, which is not shown in Fig. 12(a). The measured reflection coefficients of two ports are in agree with the simulated results, showing a −10 dB impedance bandwidth from 5.03 to 7.35 GHz and 5.09 to 7.53 GHz for Port1 and Port2, respectively, close to the simulation result of 5.13–7.39 GHz. The operating bandwidth completely covers the 5 and 6 GHz bands in Wi-Fi 6/6E protocol standard. The simulated and measured isolation is higher than 21.38 and 22.67 dB, respectively, across the matching band. The little deviations between the measured and simulated results are caused by the manual fabrication error.

B. Radiation Performance

The radiation pattern, gain, and total efficiency are measured in a standard microwave anechoic chamber. The measured and simulated maximal realized gains in the azimuth plane versus frequency are shown in Fig. 12(b). The measured realized gains of two ports are similar and slightly higher than the simulated results. The error is caused by the metal convertor which will be discussed in the next paragraph. High simulated

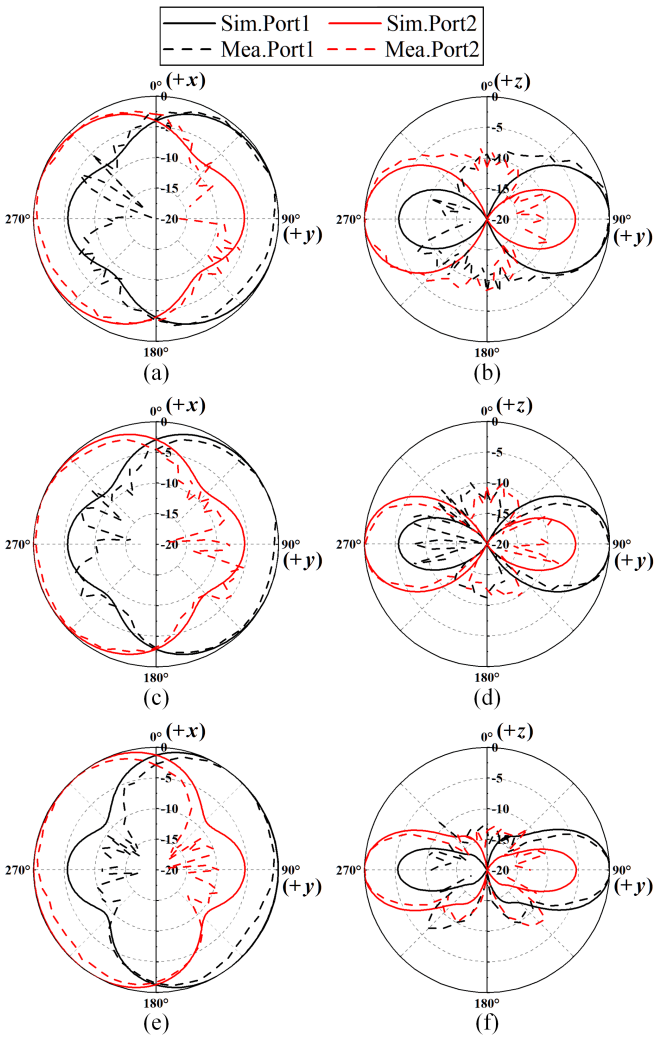

Fig. 13. Simulated and measured normalized radiation patterns. (a) E-plane and (b) H-plane at 5.2 GHz. (c) E-plane and (d) H-plane at 6 GHz. (e) E-plane and (f) H-plane at 7 GHz.

total efficiency over 95% in the whole operating band is achieved on account of the all-metal construction and good impedance matching. The measured results are over 90% of two ports which are slightly lower than the simulated result owing to the measurement errors.

Fig. 13 depicts the measured and simulated radiation patterns in the E- and H-planes at different frequencies. Although the convertor weakens the influence of the feeding cable, the metal convertor itself can also impact the radiation appreciably. Consequently, the measured radiation patterns in Fig. 13 are a little tilted with the peak gains not occurring in the front. Besides, the peak gains are a little higher than the simulated results which is caused by the reflection of the metal convertor. This explains why the measured peak gains in Fig. 12(b) are slightly higher than the simulated results. But, the measured co-polarization results still coincide well with the simulation counterparts as shown in Fig. 13. As seen, the proposed dual-antenna pair could realize an omnidirectional coverage in azimuth plane by two ports over the operating band. The measured radiation patterns in backward are not very accurate

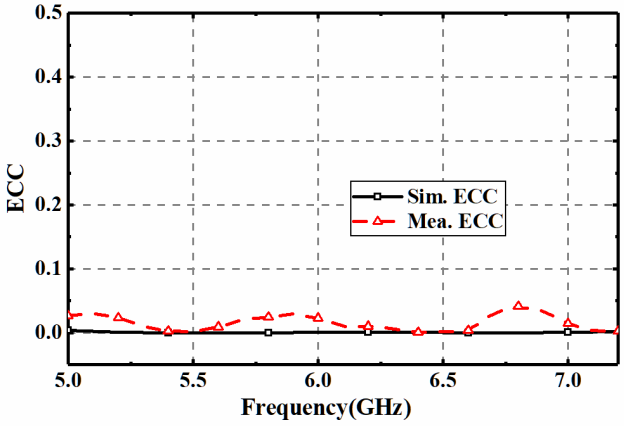

Fig. 14. Simulated and measured ECC of the dual-antenna pair.

due to the obstruction of the antenna installation pillar which stands behind the antenna in the anechoic chamber. The measured cross-polarization level at different frequencies are all lower than −15 dB, which is not shown in Fig. 13 limited by space.

To evaluate the MIMO performance of the dual-antenna pair, the simulated and measured ECCs is shown in Fig. 14. The simulated ECC is calculated by the simulated radiated far-field based on the formulation

$$\rho_e \approx |\rho_c|^2 = \left| \frac{\oiint A_{12}(\theta,\varphi)\sin\theta \mathrm{d}\theta\mathrm{d}\varphi}{\oiint A_{11}(\theta,\varphi)\sin\theta \mathrm{d}\theta\mathrm{d}\varphi \cdot \oiint A_{22}(\theta,\varphi)\sin\theta \mathrm{d}\theta\mathrm{d}\varphi} \right|^2 \quad (3)$$

where

$$A_{ij} = E_{\theta,i}(\theta,\varphi)\cdot E^*_{\theta,j}(\theta,\varphi) + E_{\varphi,i}(\theta,\varphi)\cdot E^*_{\varphi,j}(\theta,\varphi). \quad (4)$$

Here, $E_{\theta(\varphi),i}$ and $E_{\theta(\varphi),j}$ are the complex electric field of port i and port j in the elevation and azimuth planes, respectively. $()^*$ is the conjugate operator. The measured ECC is below 0.05 across the whole band demonstrating a good MIMO performance of the proposed antenna.

C. Discussion

The comparisons between the proposed dual-antenna pair and other designs for HP radiation with omnidirectional or unidirectional patterns are listed in Table III. In [21], an omnidirectional antenna based on magnetic dipole was designed. To prevent beam split, the 3rd mode is suppressed, so the bandwidth is narrow. The 1st and 3rd modes are closed by introducing vias in cavity for realizing broadband in [22], but the radiation pattern has a narrow coverage. In [23]–[25], vertical slots were excited for HP omnidirectional radiations. However, the bandwidth is narrow without covering such a wide 6 GHz band. In comparison, a wide band covering both 5 and 6 GHz bands of Wi-Fi 6/6E is achieved by our proposed dual-antenna pair. Besides, our proposed dual-antenna pair has two ports with each of them covering opposite 180° in azimuth plane, so the omnidirectional coverage is achieved. Moreover, the MIMO ability is obtained based on the different design scheme, which makes the proposed antenna

TABLE III
COMPARISON OF THE PROPOSED DUAL-ANTENNA PAIR AND PREVIOUS HP ANTENNAS

Ref.	Dimensions	Bandwidth	Radiation coverage*	MIMO
[21]	0.04 × 0.23 × 3.0	6.5%	360°	No
[22]	0.06 × 0.18 × 1.71	37.4%	≈ 90°	No
[23]	0.08 × 0.18 × 0.2	5.3% (2.4GHz band) 20% (5GHz band)	360°	No
[24]	0.7 × 0.24 × 0.24	5.8% (2.4GHz band)	360°	No
[25]	0.09 × 0.09 × 0.66	4.2% (2.4GHz band)	360°	No
This work	0.2 × 0.24 × 1.2	37.7% (5GHz+6GHz bands)	port1:180° port2:180°	Yes

* Radiation coverage is defined by the half-power beam width

more suitable for Wi-Fi router application. For example, four dipoles are necessary for a conventional router to realize 4 × 4 MIMO. In comparison, only two our proposed dual-antenna pairs are needed because the dual-antenna pair has 2 × 2 MIMO performance. Four ports have high isolation with each other and omnidirectional coverage is also realized. Besides, if adding our proposed antenna in conventional routers with only VP radiation, the channel capacity will be enhanced because of the complement of HP radiation.

V. CONCLUSION

In this article, a wideband, omnidirectional coverage, HP dual-antenna pair is proposed. By adjusting the dimensions of the OCA, the resonant frequencies of the 1st mode and the 3rd mode are closed and a wideband is obtained covering 5 GHz (5.15–5.825 GHz) and 6 GHz (5.925–7.125 GHz) bands of Wi-Fi 6/6E application. Besides, by reducing the length of the cavity, the opposite field of the 3rd mode is partly canceled out by that of the 1st mode to realize high gain HP broadside radiation without beam split. Moreover, the technique of partially sealing in the aperture reduces the dimension of the OCA effectively. AN MIMO dual-antenna pair is designed by uniting two HOCAs. The antenna pair realizes HP omnidirectional coverage in azimuth plane and the bandwidth is not affected. A high isolation over 22.67 dB across the operating band and a good ECC < 0.05 is also achieved. Therefore, the proposed dual-antenna pair could be well utilized as external antenna in routers for Wi-Fi 6/6E application. The complement of HP radiation will dramatically enhance channel capacity of conventional routers with only VP radiation.

REFERENCES

[1] M. Moosazadeh and S. Kharkovsky, "Compact and small planar monopole antenna with symmetrical L- and U-shaped slots for WLAN/WiMAX applications," *IEEE Antennas Wireless Propag. Lett.*, vol. 13, pp. 388–391, 2014.

[2] H. Chen, X. Yang, Y. Z. Yin, S. T. Fan, and J. J. Wu, "Triband planar monopole antenna with compact radiator for WLAN/WiMAX applications," *IEEE Antennas Wireless Propag. Lett.*, vol. 12, pp. 1440–1443, 2013.

[3] M. Wu and M. Chuang, "Multibroadband slotted bow-tie monopole antenna," *IEEE Antennas Wireless Propag. Lett.*, vol. 14, pp. 887–890, 2015.

[4] W.-C. Liu, C.-M. Wu, and Y.-J. Tseng, "Parasitically loaded CPW-fed monopole antenna for broadband operation," *IEEE Trans. Antennas Propag.*, vol. 59, no. 6, pp. 2415–2419, Jun. 2011.

[5] C.-Y. Pan, T.-S. Horng, W.-S. Chen, and C.-H. Huang, "Dual wideband printed monopole antenna for WLAN/WiMAX applications," *IEEE Antennas Wireless Propag. Lett.*, vol. 6, pp. 149–151, 2007.

[6] C. Chen, "A uniplanar ultrawideband antenna with unidirectional radiation for WLAN/WiMAX applications," *IEEE Antennas Wireless Propag. Lett.*, vol. 20, no. 5, pp. 743–747, May 2021.

[7] J. Gemio, G. Junkin, J. Parron, and R. Villarino, "Resonator-loaded dual-band monopole for universal WLAN," *IEEE Antennas Wireless Propag. Lett.*, vol. 8, pp. 736–739, 2009.

[8] T. Li, H. Zhai, X. Wang, L. Li, and C. Liang, "Frequency-reconfigurable bow-tie antenna for Bluetooth, WiMAX, and WLAN applications," *IEEE Antennas Wireless Propag. Lett.*, vol. 14, pp. 171–174, 2015.

[9] D. Zhao, C. Yang, M. Zhu, and Z. Chen, "Design of WLAN/LTE/UWB antenna with improved pattern uniformity using ground-cooperative radiating structure," *IEEE Trans. Antennas Propag.*, vol. 64, no. 1, pp. 271–276, Jan. 2016.

[10] J. Deng, S. Hou, L. Zhao, and L. Guo, "Wideband-to-narrowband tunable monopole antenna with integrated bandpass filters for UWB/WLAN applications," *IEEE Antennas Wireless Propag. Lett.*, vol. 16, pp. 2734–2737, 2017.

[11] W. C. Zheng, L. Zhang, Q. X. Li, and Y. Leng, "Dual-band dual-polarized compact bowtie antenna array for anti-interference MIMO WLAN," *IEEE Trans. Antennas Propag.*, vol. 62, no. 1, pp. 237–246, Jan. 2014.

[12] J. Liang, J. Hong, J. Zhao, and W. Wu, "Dual-band dual-polarized compact log-periodic dipole array for MIMO WLAN applications," *IEEE Antennas Wireless Propag. Lett.*, vol. 14, pp. 751–754, 2015.

[13] L. Liu, S. W. Cheung, and T. I. Yuk, "Compact MIMO antenna for portable UWB applications with band-notched characteristic," *IEEE Trans. Antennas Propag.*, vol. 63, no. 5, pp. 1917–1924, May 2015.

[14] S. Zhang, Z. Ying, J. Xiong, and S. He, "Ultrawideband MIMO/diversity antennas with a tree-like structure to enhance wideband isolation," *IEEE Antennas Wireless Propag. Lett.*, vol. 8, pp. 1279–1282, 2009.

[15] M. S. Khan, M. F. Shafique, A. Naqvi, A.-D. Capobianco, B. Ijaz, and B. D. Braaten, "A miniaturized dual-band MIMO antenna for WLAN applications," *IEEE Antennas Wireless Propag. Lett.*, vol. 14, pp. 958–961, 2015.

[16] X. Tang, X. Qing, and Z. N. Chen, "Simplification and implementation of decoupling and matching network with port pattern-shaping capability for two closely spaced antennas," *IEEE Trans. Antennas Propag.*, vol. 63, no. 8, pp. 3695–3699, Aug. 2015.

[17] M. Li, L. Jiang, and K. L. Yeung, "Novel and efficient parasitic decoupling network for closely coupled antennas," *IEEE Trans. Antennas Propag.*, vol. 67, no. 6, pp. 3574–3585, Jun. 2019.

[18] L. Sun, Y. Li, Z. Zhang, and H. Wang, "Antenna decoupling by common and differential modes cancellation," *IEEE Trans. Antennas Propag.*, vol. 69, no. 2, pp. 672–682, Feb. 2021.

[19] Y. He, Y. Li, L. Zhu, and P.-Y. Chen, "Miniaturization of omnidirectional cavity antennas using substrate-integrated impedance surfaces," *IEEE Trans. Antennas Propag.*, vol. 69, no. 3, pp. 1728–1733, Mar. 2021.

[20] Z. Zhou, Y. Li, Y. He, Z. Zhang, and P.-Y. Chen, "A slender Fabry–Perot antenna for high-gain horizontally polarized omnidirectional radiation," *IEEE Trans. Antennas Propag.*, vol. 69, no. 1, pp. 526–531, Jan. 2021.

[21] Z. Liang, Y. Li, X. Feng, J. Liu, J. Qin, and Y. Long, "Microstrip magnetic monopole and dipole antennas with high directivity and a horizontally polarized omnidirectional pattern," *IEEE Trans. Antennas Propag.*, vol. 66, no. 3, pp. 1143–1152, Mar. 2018.

[22] Y. Shi and J. Liu, "Investigation of a via-loaded microstrip magnetic dipole antenna with enhanced bandwidth and gain," *IEEE Trans. Antennas Propag.*, vol. 67, no. 7, pp. 4836–4841, Jul. 2019.

[23] J. Guo, H. Bai, A. Feng, Y. Liu, Y. Huang, and X. Zhang, "A compact dual-band slot antenna with horizontally polarized omnidirectional radiation," *IEEE Antennas Wireless Propag. Lett.*, vol. 20, no. 7, pp. 1234–1238, Jul. 2021.

[24] P. Liu, Z. Meng, L. Wang, Y. Zhang, and Y. Li, "Omnidirectional dual-polarized saber antenna with low wind drag," *IEEE Trans. Antennas Propag.*, vol. 68, no. 1, pp. 558–563, Jan. 2020.

[25] Y. Li, Z. Zhang, J. Zheng, and Z. Feng, "Compact azimuthal omnidirectional dual-polarized antenna using highly isolated colocated slots," *IEEE Trans. Antennas Propag.*, vol. 60, no. 9, pp. 4037–4045, Sep. 2012.

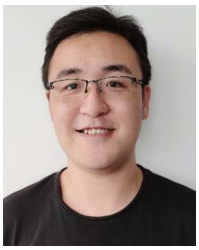

Xiaopeng Zhang received the B.S. degree from Xidian University, Xi'an, China, in 2019. He is currently pursuing the Ph.D. degree with the Department of Electrical and Engineering, Tsinghua University, Beijing, China.

His current research interests include leaky-wave antennas, antenna decoupling, and MIMO.

Libin Sun (Member, IEEE) received the B.S. degree from Xidian University, Xi'an, China, in 2016, and the Ph.D. degree in electronic engineering from Tsinghua University, Beijing, China, in 2021.

He is currently working for the Consumer Business Group, Huawei Technologies Company, Ltd., Shanghai, as a Senior Antenna Engineer. He has authored or coauthored over 15 journal articles and holds five granted Chinese patents. His current research interests include antenna design and electromagnetic theory, particularly in 5G mobile phone antennas, antenna decoupling techniques and MIMO antennas, millimeter-wave antennas, and interaction effects between antenna and human body.

Dr. Sun was a recipient of the Top Reviewer Award for the IEEE TRANSACTIONS ON ANTENNAS AND PROPAGATION in 2019, the Honorable Mention in 2020 IEEE AP-S Student Paper Competition, the Chinese National Doctorial Scholarship in 2019, and the Principal Scholarship (Highest Honor) of Tsinghua University in 2020. He has served as the Session Chair for the APMC 2020 and serves as a Reviewer for several international academic journals such as the IEEE TRANSACTIONS ON ANTENNAS AND PROPAGATION, IEEE ANTENNAS AND WIRELESS PROPAGATION LETTERS, IEEE ACCESS, IET *Microwaves, Antennas & Propagation, IET Electronics Letters*, and *Microwave and Optical Technology Letters*.

Yue Li (Senior Member, IEEE) received the B.S. degree in telecommunication engineering from Zhejiang University, Zhejiang, China, in 2007, and the Ph.D. degree in electronic engineering from Tsinghua University, Beijing, China, in 2012.

He is currently an Associate Professor with the Department of Electronic Engineering, Tsinghua University, where he was a Postdoctoral Fellow in June 2012. In December 2013, he was a Research Scholar with the Department of Electrical and Systems Engineering, University of Pennsylvania, Philadelphia, PA, USA. He was also a Visiting Scholar with the Institute for Infocomm Research (I2R), A*STAR, Singapore, in 2010, and Hawaii Center of Advanced Communication (HCAC), University of Hawaii at Manoa, Honolulu, HI, USA, in 2012. Since January 2016, he has been with Tsinghua University, where he is an Assistant Professor. He has authored and coauthored over 170 journal articles and 50 international conference papers, and holds 25 granted Chinese patents. His current research interests include metamaterials, plasmonics, electromagnetics, nanocircuits, mobile and handset antennas, MIMO and diversity antennas, and millimeter-wave antennas and arrays.

Dr. Li was a recipient of the Issac Koga Gold Medal from URSI General Assembly in 2017; the Second Prize of Science and Technology Award of China Institute of Communications in 2017; the Young Scientist Awards from the conferences of PIERS 2019, ACES 2018, AT-RASC 2018, AP-RASC 2016, EMTS 2016, URSI GASS 2014. He is serving as the Associate Editor of IEEE TRANSACTIONS ON ANTENNAS AND PROPAGATION, IEEE ANTENNAS AND WIRELESS PROPAGATION LETTERS, *Microwave and Optical Technology Letters*, *Computer Applications in Engineering Education*, and as the Editorial Board of Scientific Report, MDPI Sensors, and MDPI Electronics.

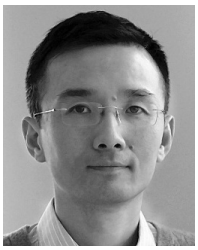

Zhijun Zhang (Fellow, IEEE) received the B.S. and M.S. degrees from the University of Electronic Science and Technology, Chengdu, China, in 1992 and 1995, respectively, and the Ph.D. degree from Tsinghua University, Beijing, China, in 1999.

In 1999, he was a Postdoctoral Fellow with the Department of Electrical Engineering, University of Utah, where he was appointed a Research Assistant Professor in 2001. In May 2002, he was an Assistant Researcher with the University of Hawaii at Manoa, Honolulu, HI, USA. In November 2002, he joined Amphenol T&M Antennas, Vernon Hills, IL, as a Senior Staff Antenna Development Engineer and was then promoted to the position of Antenna Engineer Manager. In 2004, he joined Nokia Inc., San Diego, CA, as a Senior Antenna Design Engineer. In 2006, he joined Apple Inc., Cupertino, CA, as a Senior Antenna Design Engineer and was then promoted to the position of Principal Antenna Engineer. Since August 2007, he has been with Tsinghua University, where he is a Professor in the Department of Electronic Engineering. He is the author of Antenna Design for Mobile Devices (Wiley, 1st ed. 2011, 2nd ed. 2017). He served as Associate Editor of the IEEE TRANSACTIONS ON ANTENNAS AND PROPAGATION (2010–2014) and the IEEE ANTENNAS AND WIRELESS PROPAGATION LETTERS (2009–2015).